

Integrated Ferroelectrics

An International Journal

ISSN: (Print) (Online) Journal homepage: <https://www.tandfonline.com/loi/ginf20>

The Electrical Performances and Leakage Current Conduction Mechanism of $\text{Al}_2\text{O}_3/\text{ZrO}_2/\text{SiO}_2/\text{ZrO}_2/\text{Al}_2\text{O}_3$ MIM Capacitors

Q. X. Zhang

To cite this article: Q. X. Zhang (2021) The Electrical Performances and Leakage Current Conduction Mechanism of $\text{Al}_2\text{O}_3/\text{ZrO}_2/\text{SiO}_2/\text{ZrO}_2/\text{Al}_2\text{O}_3$ MIM Capacitors, Integrated Ferroelectrics, 217:1, 233-239, DOI: [10.1080/10584587.2021.1911316](https://doi.org/10.1080/10584587.2021.1911316)

To link to this article: <https://doi.org/10.1080/10584587.2021.1911316>



Published online: 21 Jul 2021.



Submit your article to this journal [↗](#)



Article views: 11



View related articles [↗](#)



View Crossmark data [↗](#)



The Electrical Performances and Leakage Current Conduction Mechanism of $\text{Al}_2\text{O}_3/\text{ZrO}_2/\text{SiO}_2/\text{ZrO}_2/\text{Al}_2\text{O}_3$ MIM Capacitors

Q. X. Zhang

Shanghai Technical Institute of Electronics & Information, Shanghai, China

ABSTRACT

In this paper, we prepared the $\text{Al}_2\text{O}_3/\text{ZrO}_2/\text{SiO}_2/\text{ZrO}_2/\text{Al}_2\text{O}_3$ (AZSZA) metal-insulator-metal (MIM) capacitors by atomic-layer-deposition technique. By increasing the thickness of SiO_2 from 0 nm to 3 nm, the quadratic capacitance voltage coefficients improved significantly from 2130 ppm/V^2 to -121 ppm/V^2 because of the offsetting effects of ZrO_2 and SiO_2 dielectric. Meanwhile, for our interested $\text{SiO}_2=3 \text{ nm}$ sample, the capacitance density is $7.40 \text{ fF}/\mu\text{m}^2$ and the leakage current density is $3.08 \times 10^{-8} \text{ A/cm}^2$ at 5 V. We also studied the leakage current conduction mechanism of AZSZA dielectric MIM capacitors and found that at high field the conduction mechanism was dominated by Poole Frenkel emission.

ARTICLE HISTORY

Received 8 November 2020
Accepted 15 February 2021

KEYWORDS

$\text{Al}_2\text{O}_3/\text{ZrO}_2/\text{SiO}_2/\text{ZrO}_2/\text{Al}_2\text{O}_3$; MIM capacitors; Poole Frenkel emission

1. Introduction

Metal–insulator–metal (MIM) capacitors are essential to integrated circuits (ICs). They can be used in many ways, such as decoupling and filtering. High capacitance density, low leakage current and small quadratic voltage coefficient of capacitance (α) are signals of good electrical performances of MIM capacitors. In order to get high capacitance density, high dielectric constant (k) materials such as Ta_2O_5 , HfO_2 , Al_2O_3 , TiO_2 and ZrO_2 [1–4] can be used. ZrO_2 thin film is considered to be a strong candidate among these high k materials to replace traditional dielectric materials SiO_2 and Si_3N_4 because it has many advantages, for instance, high breakdown electric field, high dielectric constant and large energy gap width [4].

Someone has studied a single ZrO_2 dielectric MIM capacitors and high capacitance density is obtained, but the leakage current and α value are poor [5]. Here, we introduced the Al_2O_3 and SiO_2 layers to improve the foregoing two parameters because Al_2O_3 has a large band gap of $\sim 8.8 \text{ eV}$ and SiO_2 has a negative α value, so the $\text{Al}_2\text{O}_3/\text{ZrO}_2/\text{SiO}_2/\text{ZrO}_2/\text{Al}_2\text{O}_3$ (AZSZA) structure MIM capacitors were designed. What needs to be emphasized is that the AZSZA structure was prepared in the same Atomic Layer Deposition (ALD) system. This not only decreases the complexity and cost of the experiment, but also decreases the probability of contamination and introduction of impurities. Therefore, it is a better method to grow all the dielectric materials in the

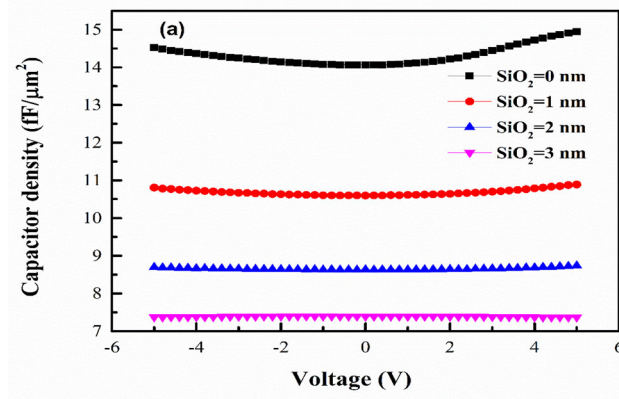


Figure 1. Typical capacitance–voltage (C–V) characteristics of the AZSZA MIM capacitors at 100 kHz.

same chamber. The reason for using ALD technology is that it has many advantages [6], such as low temperature process, precise thickness control and large area deposition uniformity .

2. Experimental

Firstly, the ~ 150 nm TaN thin films were sputtered as a bottom electrode on Si substrate coated with ~ 500 nm oxide film. Secondly, the Si substrate coated with TaN bottom electrode was placed into the ALD chamber to deposit $\text{Al}_2\text{O}_3/\text{ZrO}_2/\text{SiO}_2/\text{ZrO}_2/\text{Al}_2\text{O}_3$ (AZSZA) nanolaminates. In order to research the effects of the thickness of SiO_2 film on the performance of AZSZA MIM capacitors, the thicknesses of SiO_2 varies from 0 to 3 nm, increase 1 nm every time. Meanwhile the individual thickness of Al_2O_3 and ZrO_2 layers were optimized at 1 nm and 7 nm, respectively. After assembly of the above stacked insulator, the sputtered ~ 150 nm TaN top electrodes were formed and defined by photolithography and dry etching. Capacitance-voltage (C-V) characteristic were measured by Agilent 4294 A at 100 kHz and the current-voltage (I-V) measurement was performed by Agilent B1500A equipment.

3. Results and Discussion

Figure 1 is the C-V characteristics of the AZSZA MIM capacitors. The four samples were labeled as $\text{SiO}_2=0$ nm, $\text{SiO}_2=1$ nm, $\text{SiO}_2=2$ nm, and $\text{SiO}_2=3$ nm. It can be seen from the graph, with the increase of SiO_2 thickness, the capacitance density decreased gradually. The corresponding capacitance density is 14.06, 10.60, 8.64 and 7.40 $\text{fF}/\mu\text{m}^2$ at 0 V for $\text{SiO}_2 = 0, 1, 2, 3$ nm samples, and the calculated k values are 25.4, 20.4, 17.6 and 15.9 respectively. The occurrence of high k value is due to the appearance of ZrO_2 crystal layer [7]. The decrease of capacitance density is due to the increase of SiO_2 and the small k value of SiO_2 , which only 3.9. Therefore, even if the increase of SiO_2 is only 1 nm, the change of capacitance density is also obvious.

Small α is vital for the application of MIM capacitors, for it denotes the variation of capacitance with applied voltage. It can be described by $C(V)=C_0(\alpha V^2+\beta V+1)$. Here,

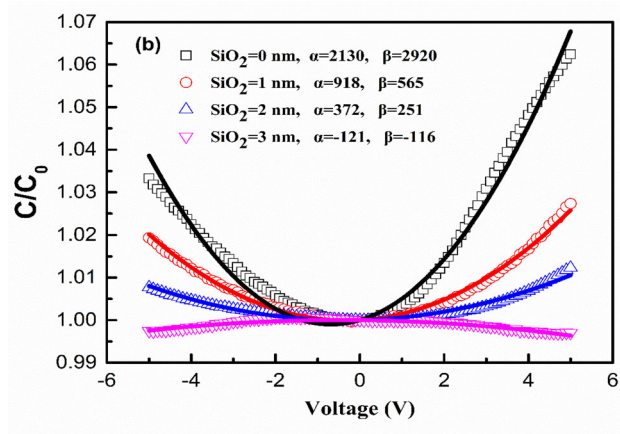


Figure 2. The curves of normalized capacitance and voltage for the MIM capacitors of four samples.

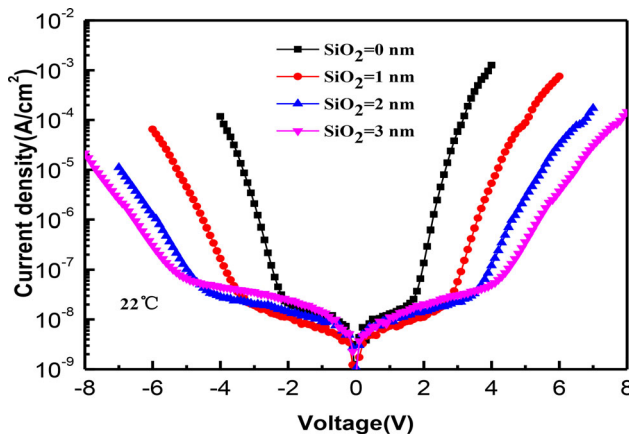


Figure 3. The current density–voltage (J - V) characteristics at room temperature of the four samples.

C_0 represents the capacitance density at zero bias, α and β are the quadratic and linear capacitance voltage coefficients, which can be obtained by fitting the curve of normalized capacitance–voltage according to the quadratic equation. Figure 2 is the curve of normalized capacitance and voltage for the MIM capacitors of the four samples. A strong positive parabolic curve can be seen for the $\text{SiO}_2=0\text{ nm}$ sample. With the increase of SiO_2 thickness, the capacitance voltage coefficient has been improved because of the negative α of SiO_2 , which can neutralize with the positive α of ZrO_2 . When $\text{SiO}_2=3\text{ nm}$, we can see a parabola going downwards and relatively flat, indicating that α value becomes negative and the value is small. It should be emphasized that if the thickness of SiO_2 is adjusted at $2\sim 3\text{ nm}$, the α value will continue to decrease until it gets to zero [8].

The current density–voltage (J - V) characteristics of the four samples are shown in Figure 3. It is obviously that the current density gradually decreases with the increase of SiO_2 thickness. For the sample of the $\text{SiO}_2 = 3\text{ nm}$, the leakage current density is $1.57 \times 10^{-8}\text{ A/cm}^2$ at -2 V , which is lower than that of $\text{TiO}_2/\text{SiO}_2$ [9], $\text{SiO}_2/\text{ZrO}_2$ [10] and HfO_2 [11] MIM capacitors. Even at 5 V for the $\text{SiO}_2=3\text{ nm}$ sample, the leakage

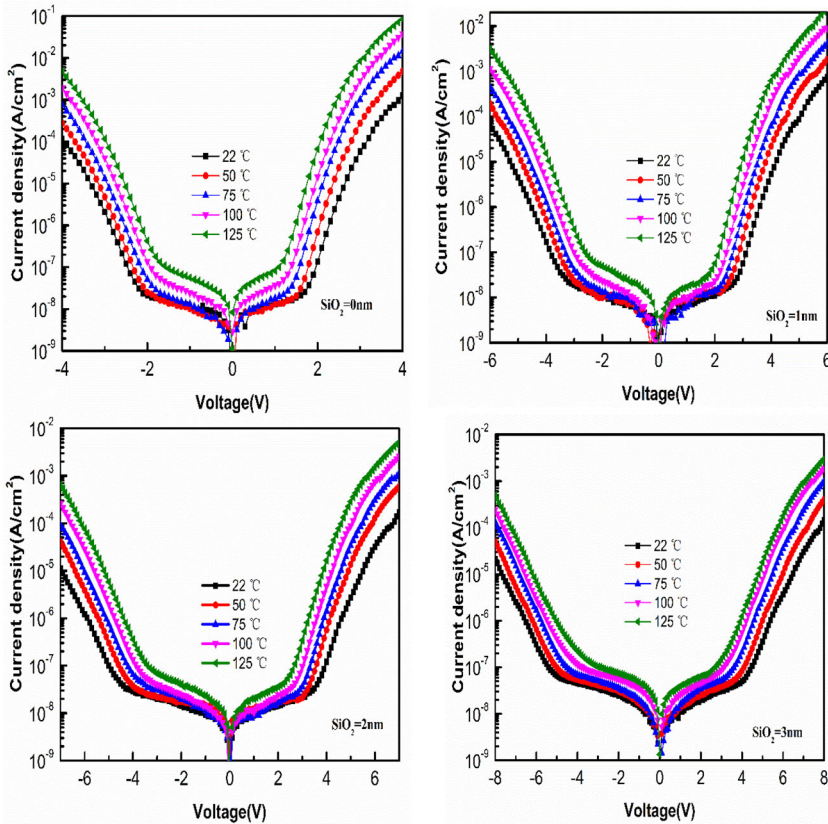


Figure 4. The current density–voltage (J–V) characteristics at different temperatures of the four samples.

current density is only $3.08 \times 10^{-8} \text{ A/cm}^2$. If the components of AZSZA MIM capacitor are continuously adjusted, its current density can be further optimized, as proposed by Kukli et al. [12].

Although some groups have observed the ZrO_2 -based dielectric MIM capacitors [4, 5, 13], few researchers have explored their leakage current mechanisms. Figure 4 illustrates the current density–voltage characteristics for the four samples AZSZA MIM capacitors, which were measured at 22, 50, 75, 100 and 125 °C in order to observe the leakage current mechanism. It can be seen that for the four samples, the influence of temperature on the current at low field is not significant, because in low field the current is mostly trap assisted tunneling current [14, 15]. While at high field, the current is obviously increased with the increase of temperature, so we will mainly study the leakage current density at high field.

Poole–Frenkel (PF) emission often occurs in high temperature and high field [16], which can be expressed by Eq(1).

$$J = AE \exp \left[\frac{-q \left(\phi_t - \sqrt{qE/\pi\epsilon_0\epsilon_r} \right)}{kT} \right] \tag{1}$$

Where A is a constant, q, E, T and k denote the electronic charge, the electric field, the absolute temperature, and the Boltzmann constant, respectively. ϵ_r and ϵ_0 represent

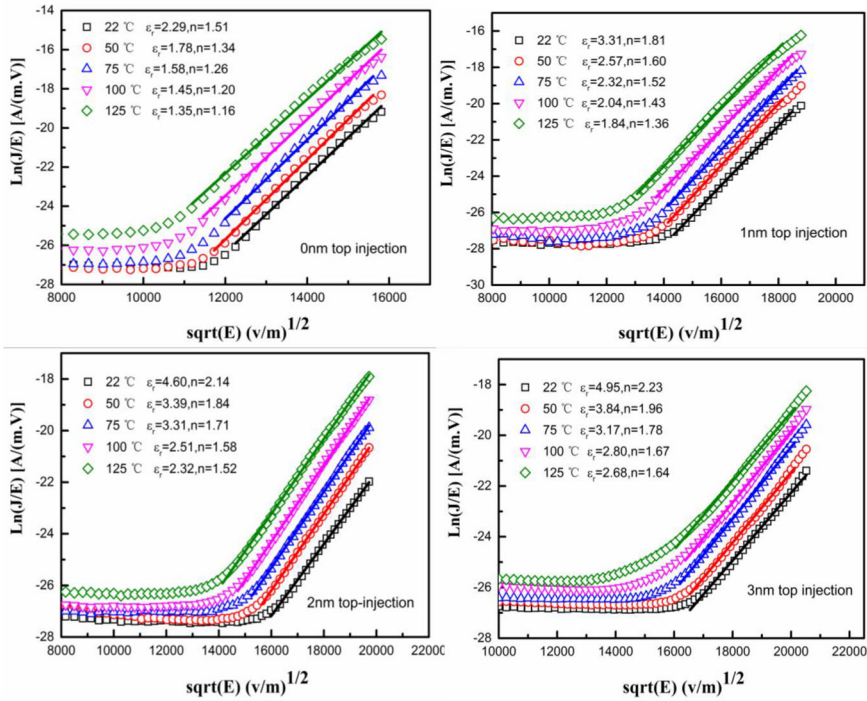


Figure 5. Typical plotting of $\ln(J/E)$ vs $E^{1/2}$ in the high field range according to the PF emission.

the dynamic dielectric constant of the dielectric layer and the permittivity of free space. ϕ_t signifies the energy barrier separating the traps from the conduction band.

If the leakage mechanism is PF emission, it should meet two conditions. One is that $\ln(J/E)$ and $E^{1/2}$, as well as $\ln J$ and $1/T$ will satisfy the linear relationship. The other is the dynamic dielectric constant of the dielectric layer ϵ_r should close to square of the refractive index ($\epsilon_r \approx n^2$). Since our structure is symmetrical, the leakage mechanism should be the same. According to the above idea, the top injection temperature curve of the four samples was calculated and fitted to verify the mechanism. Figure 5 is the relationship plot of $\ln(J/E)$ and $E^{1/2}$ in the high field region. It is evident that linear relationships are obtained at different temperatures. From the slope of the fitted straight line of the four samples at 22, 50, 75, 100 and 125 °C, We extracted ϵ_r values and they are shown in the figure, which are very close to square of the refractive index ($\epsilon_r \sim n^2$). Furthermore, the relationship plots between $\ln(J)$ and $1/T$ of our samples were displayed in Figure 6. Based on the slope of the fitted straight line, the ϕ_t are also calculated by introducing $\epsilon_r = 2.29, 3.31, 4.60$ and 4.95 for the four samples, as shown in Figure 6. All these results indicate that in the high field region the leakage current mechanism for AZSZA MIM capacitors is PF emission.

4. Conclusion

To summarize, AZSZA dielectric MIM capacitors were prepared by full ALD technique. The SiO_2 thickness has great impacts on the electrical performance of AZSZA MIM capacitors. For the $\text{SiO}_2 = 3\text{nm}$ sample we are interested in, it has shown large capacitance density, small α value and extremely low leakage current density. And through

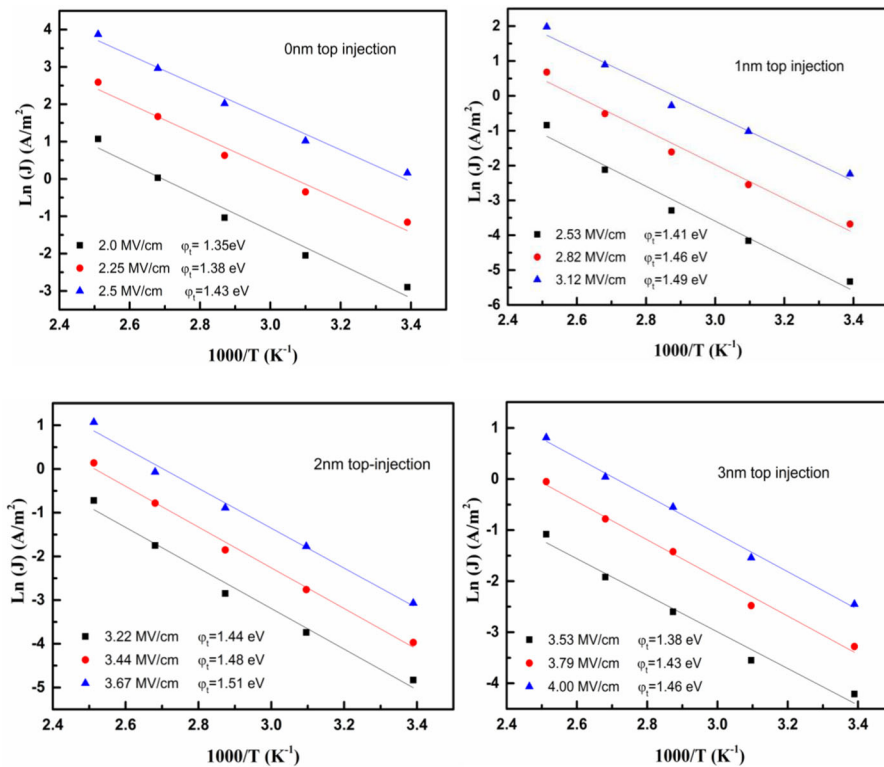


Figure 6. Plotting of $\ln(J)$ vs $1/T$ of the four samples, and the corresponding ϕ_t are also extracted.

discussion we found that at high field region the leakage conduction mechanism of AZSZA structure is PF emission.

References

1. T. Ishikawa *et al.*, High-capacitance Cu/Ta₂O₅/Cu MIM structure for SoC applications featuring a Single- Mask Add-on Process. *IEDM Tech. Dig.*, 2002 940–942.
2. H. Hu *et al.*, MIM capacitors using atomic-layer-deposited high-k (HfO₂)_{1-x}(Al₂O₃)_x dielectrics, *IEEE Electron Device Lett* **24**, 60 (2003). DOI: [10.1109/LED.2002.807703](https://doi.org/10.1109/LED.2002.807703).
3. Y. H. Wu *et al.*, MIM capacitors with crystalline-TiO₂/SiO₂ stack featuring high capacitance density and low voltage coefficient, *IEEE Electron Device Lett.* **33** (1), 104 (2012). DOI: [10.1109/LED.2011.2173791](https://doi.org/10.1109/LED.2011.2173791).
4. T. Bertaud *et al.*, Frequency effect on voltage linearity of ZrO₂-based RF metal–insulator–metal capacitors, *Electron Device Letters, IEEE* **31** (2010).
5. C. Y. Tsai *et al.*, Improved capacitance density and reliability of high- κ Ni/ZrO₂/TiN MIM capacitors using laser-annealing technique, *IEEE Electron Device Lett.* **31** (7), 749 (2010). DOI: [10.1109/LED.2010.2049636](https://doi.org/10.1109/LED.2010.2049636).
6. S. J. Ding *et al.*, Metal-insulator-metal capacitors using atomic-layer-deposited Al₂O₃/HfO₂/Al₂O₃ sandwiched dielectrics for wireless communications, *J. Vac. Sci. Technol. B.* **24** (6), 2518 (2006). DOI: [10.1116/1.2357746](https://doi.org/10.1116/1.2357746).
7. B.-Z. Qiu-Xiang Zhang *et al.*, Full ALD Al₂O₃/ZrO₂/SiO₂/ZrO₂/Al₂O₃ stacks for high-performance MIM capacitors, *IEEE Electron Device Lett* **35**, 1121 (2014). DOI: [10.1109/LED.2014.2359195](https://doi.org/10.1109/LED.2014.2359195).

8. The International Technology Roadmap for Semiconductors. [Online] 2013 Available: <http://www.itrs.net/>.
9. J. R. Wu *et al.*, Effect of nitrogen passivation on the performance of MIM capacitors with a crystalline-TiO₂/SiO₂ stacked insulator, *IEEE Electron Device Lett.* **33** (6), 878 (2012). DOI: [10.1109/LED.2012.2192253](https://doi.org/10.1109/LED.2012.2192253).
10. S. D. Park *et al.*, Bulk and interface effects on voltage linearity of ZrO₂-SiO₂ multilayered metal-insulator-metal capacitors for analog mixed-signal applications, *Appl. Phys. Lett.* **95** (2), 022905 (2009). DOI: [10.1063/1.3182856](https://doi.org/10.1063/1.3182856).
11. X. Yu *et al.*, A high-density MIM capacitor (13 fF/μm²) using ALD HfO₂ dielectrics, *IEEE Electron Device Lett.* **24**, 63 (2003). DOI: [10.1109/LED.2002.808159](https://doi.org/10.1109/LED.2002.808159).
12. K. Kukli *et al.*, Tailoring the dielectric properties of HfO₂-Ta₂O₅ nanolaminates, *Appl. Phys. Lett.* **68** (26), 3737 (1996). DOI: [10.1063/1.115990](https://doi.org/10.1063/1.115990).
13. W. Weinreich *et al.*, Detailed leakage current analysis of metal-insulator-metal capacitors with ZrO₂, ZrO₂/SiO₂/ZrO₂, and ZrO₂/Al₂O₃/ZrO₂ as dielectric and TiN electrodes, *Journal of Vacuum Science & Technology B: Microelectronics and Nanometer Structures* **31** (1), 01A109 (2013). DOI: [10.1116/1.4768791](https://doi.org/10.1116/1.4768791).
14. X. R. Cheng, Y. C. Cheng, and B. Y. Liu, Nitridation-enhanced conductivity behavior and current transport mechanism in thin thermally nitrided SiO₂, *J Appl Phys* **63** (3), 797 (1988). DOI: [10.1063/1.340072](https://doi.org/10.1063/1.340072).
15. E. Suzuki, D. K. Schroder, and Y. Hayashi, Carrier conduction in ultrathin nitrided oxide films, *J Appl Phys* **60** (10), 3616 (1986). DOI: [10.1063/1.337568](https://doi.org/10.1063/1.337568).
16. F. C. Chiu, C. Y. Lee, and P. Tung-Ming, Current conduction mechanisms in Pr₂O₃/oxynitride laminated gate dielectrics, *J Appl Phys* **105** (7), 074103 (2009). DOI: [10.1063/1.3103282](https://doi.org/10.1063/1.3103282).